Linking reduced breaking crest speeds to unsteady nonlinear water wave group behavior

M.L. Banner[1]*, X. Barthelemy[1,2], F. Fedele[3], M. Allis[2], A. Benetazzo[4], F. Dias[5] and W.L. Peirson[2].

1. School of Mathematics and Statistics, The University of New South Wales, Sydney 2052, Australia

2. Water Research Laboratory, School of Civil and Environmental Engineering, The University of New South Wales, Manly Vale, NSW 2093, Australia

3. School of Civil and Environmental Engineering, and School of Electrical and Computer Engineering, Georgia Institute of Technology, Atlanta, GA 30332, USA.

4. Institute of Marine Sciences, National Research Council (CNR-ISMAR), Venice, Italy.

5. UCD School of Mathematical Sciences, University College Dublin, Belfield, Dublin 4, Ireland.

Abstract

Observations show that maximally-steep breaking water wave crest speeds are much slower than expected. We report a wave-crest slowdown mechanism generic to *unsteady* propagating deep water wave groups. Our fully nonlinear computations show that just prior to reaching its maximum height, each wave crest slows down significantly and either breaks at this reduced speed, or accelerates forward unbroken. This finding is validated in our extensive laboratory and field observations. This behavior appears to be generic to unsteady dispersive wave groups in other natural systems.

Introduction

Nonlinear wave groups occur in a wide range of natural systems, exhibiting complex behaviors especially in focal zones where there is rapid wave energy concentration and possible ‘wave-breaking’. The incompletely-understood interplay between dispersion, directionality and nonlinearity presents a significant knowledge gap presently beyond analytical treatment. Here, we investigate maximally-steep, deep-water wave group behaviour, but the findings appear relevant to dispersive nonlinear wave motion in many other natural systems.

In the open ocean, wind forcing generates waves that can steepen and break conspicuously as whitecaps, strongly affecting fundamental air-sea exchanges, including greenhouse gases. This has stimulated recent interest in measuring whitecap properties spectrally. While accurately measuring wavelengths of individual breakers is difficult, measuring whitecap *speeds* can provide a less direct but more convenient method: since a whitecap remains attached to the underlying wave crest during active breaking. The dispersion relation from Stokes' classical deep water wave theory discussed below (Stokes [1]) conventionally provides the wavelength from the observed whitecap speed (Phillips [2]).

Stokes' theory was developed for a *steady*, uniform train of two-dimensional (2D) non-linear, deep-water waves of small-to-intermediate mean steepness ak (=2π×amplitude/wavelength), for which the intrinsic wave speed c increases slowly with ak:

$$c = c_0[1+1/2\ (ak)^2+\text{higher order terms in } (ak)]^{1/2} \quad (1)$$

where c_0 is the wave speed for linear (infinitesimally-steep) waves. Extending (1) computationally to maximally-steep, steady waves (Longuet-Higgins [3]), c approaches $1.1c_0$. Thus, increased wave steepness has long been associated with *higher* wave speeds.

Natural wind-waves comprise a spectrum of modes interacting on different scales, producing evolving wave-group patterns rather than steady, uniform wavetrains (Longuet-Higgins [4]). Here we investigate the 'dominant' waves, i.e. those with the largest spectral amplitudes after filtration of higher-wavenumber components. Within a group, each advancing dominant wave gradually changes its height and shape, characterized by slow forward and backward leaning of the crests (Tayfun [5]), also transiently becoming the tallest wave. This tallest wave may break, or else decrease in height while advancing unbroken towards the front of the group.

In this context, previous deep-water breaking wave laboratory studies (Rapp and Melville [6]; Stansell and McFarlane [7]; Jessup and Phadnis [8]) suggest that breaking-crest speeds are typically O(20%)

lower than expected from linear-wave theory, contrary to the expectation from (1) that steeper breaking waves should propagate faster. Understanding this paradoxical crest slowdown behaviour is central to both refining present knowledge on water-wave propagation and dynamics, and optimal implementation of Phillips' spectral framework for breaking waves (Phillips [2]; Kleiss and Melville [9]; Gemmrich et al. [10]).

Historically, an appreciable literature has developed on non-breaking, focusing, deep-water, nonlinear wave packets. However, only the studies of Johannessen and Swan ([11], [12]) identified crest slowdown at focus, reporting an O(10%) crest-speed slowdown relative to its linear-theory prediction. To understand the underlying physics, the present study investigates how very steep unsteady, non-periodic, deep-water wave groups propagate when frequently-assumed theoretical constraints are relaxed, including steady-state, spatially-uniform or slowly-varying, weakly-nonlinear wavetrain behavior. Our goal was to investigate initial breaker speeds, hence it was crucial to track changes, up to the point of breaking initiation, in dominant wave-crest speeds within evolving nonlinear wave groups.

Methodology and results

No presently-available analytic theory can predict the evolution of fully-nonlinear, deep-water wave groups. Our primary research strategy utilized simulations from a fully-nonlinear, 3D numerical wave code, validated against results from our innovative laboratory and ocean-wave observations.

Our simulations were generated using a numerical wave tank (Grilli et al. [13]). This boundary element code simulates fully-nonlinear potential flow theory and is able to model extreme water waves to the point of overturning. A programmable wave paddle produces a specific 2D or 3D chirped wave-group structure comprising a prescribed number of carrier waves with given initial amplitudes, wavenumbers, frequencies and phases. This shapes the spatial and temporal bandwidths characterizing the group structure and its spectrum. For the simulations, including the 2D example below, the paddle followed the displacement-motion equation (3) described in Song and Banner [14], with N=5, 7 and 9. We also investigated corresponding laterally-converging 3D chirped packet cases with 10- and 25-wavelength focal distances. In this study, breaking occurred predominantly as sequential spilling events with occasional local plunging. The complementary wave-basin experiments described below also included comparable bimodal, modulating nonlinear wave packets specified by equation (2) in [14]. The half-power bandwidths were O(8) times broader than investigated in [9].

Figure 1(a) shows the complex growth behavior experienced by all dominant wave crests evolving within a representative 2D nonlinear, non-breaking wave group. The initial steepest wave decays and is replaced by the following growing wave, which grows modestly, then slows down and is replaced by the annotated faster-growing crest, which evolves to its maximum height and decays. As each new crest develops, it grows (A-B-C) then slows down and attenuates (C-D), then accelerates (D-E) back to its original speed while advancing towards the front of the group.

Figure 1(b) shows the spatial wave profile in greater detail at the evolution times A-E in Figure 1(a). The dominant wave grows asymmetrically, initially leaning forward as it steepens within the group. In the absence of breaking, the steepest wave advances leaning forward, relaxing back to symmetry near its maximum height (the focal point), then leans backwards past the maximum elevation. Forward-leaning crests are accompanied by backward leaning troughs, and vice-versa. This leaning is a *generic* feature of each crest in natural, unsteadily-evolving dispersive nonlinear water wave groups (Tayfun [5]).

Relative to the speed of a classical (symmetrical) Stokes wave, significant crest (and trough) speed changes accompany the leaning, measured by tracking the (horizontal) speed of a given wave-crest profile in space and time. The generic crest-speed slowdown is identified in Figure 1(c) by the steeper slope of the displacement-time curve between B and D relative to the indicated *linear* wave trajectory (speed c_0), where c_0 is the speed of the spectral peak determined from the computed wave-packet dispersion relation. The actual speed reduction relative to c_0 is 18%. This lasts about one wave period, with a spatial extent of about one wavelength. Figure 1(d) shows a typical trajectory when crest speed is plotted against local crest steepness $s_c=a_ck_c$, where a_c is the time-dependent crest height above mean-water level and the corresponding local wavenumber k_c is defined as π divided by the local zero-crossing separation spanning the given crest. Introducing s_c was necessary to describe the complexity of *unsteady* nonlinear wave crest behaviour, and was easily computed for Stokes waves for the crest-speed comparison shown.

The significant departure of the crest speed versus crest steepness trajectory for waves in unsteady wave groups compared with the classical Stokes for steady wavetrain prediction underpins the central findings in this study. In this example, the maximum crest steepness marginally precedes the slowest crest speed, with the trajectory looping counter-clockwise about this point. This trajectory is not generic, since other simulated cases and the experimental curve of Figure 2(b) below showed clockwise looping. Further studies are needed to explain this effect. Also, as seen in Figure 1(d), the asymmetry of the dominant wave shape near its maximum steepness results in different crest speeds for growing and decaying crests of the same steepness. Note that the local peak in crest speed between A and B at $s_c \approx 0.2$ is an artefact of our crest-tracking algorithm, resulting from the complex crest transition seen in Figure 1(a) at (x/L~4, t/T~13.5) when the detected crest location jumps abruptly from the receding crest to the newly-developing crest.

The above discussion was for 2D waves, but laterally-focused (3D) wave fronts in both our simulations and wave-basin investigation (described below) show similar leaning and crest-slowdown behavior, with the subsequent breaker-crest speed initiated at ~$0.8c_0$.

Relative to classical ocean-wave speeds, our model results for the speeds of the left-hand and right-hand zero-crossings spanning the tallest wave shows that their average remains close to the linear wave speed c_0 (Fig. 1(c)), with modest local fluctuations of (+7% to -1%). Hence, aside from the strong unsteady leaning crest and trough motions, the waves propagate largely as expected from Stokes theory.

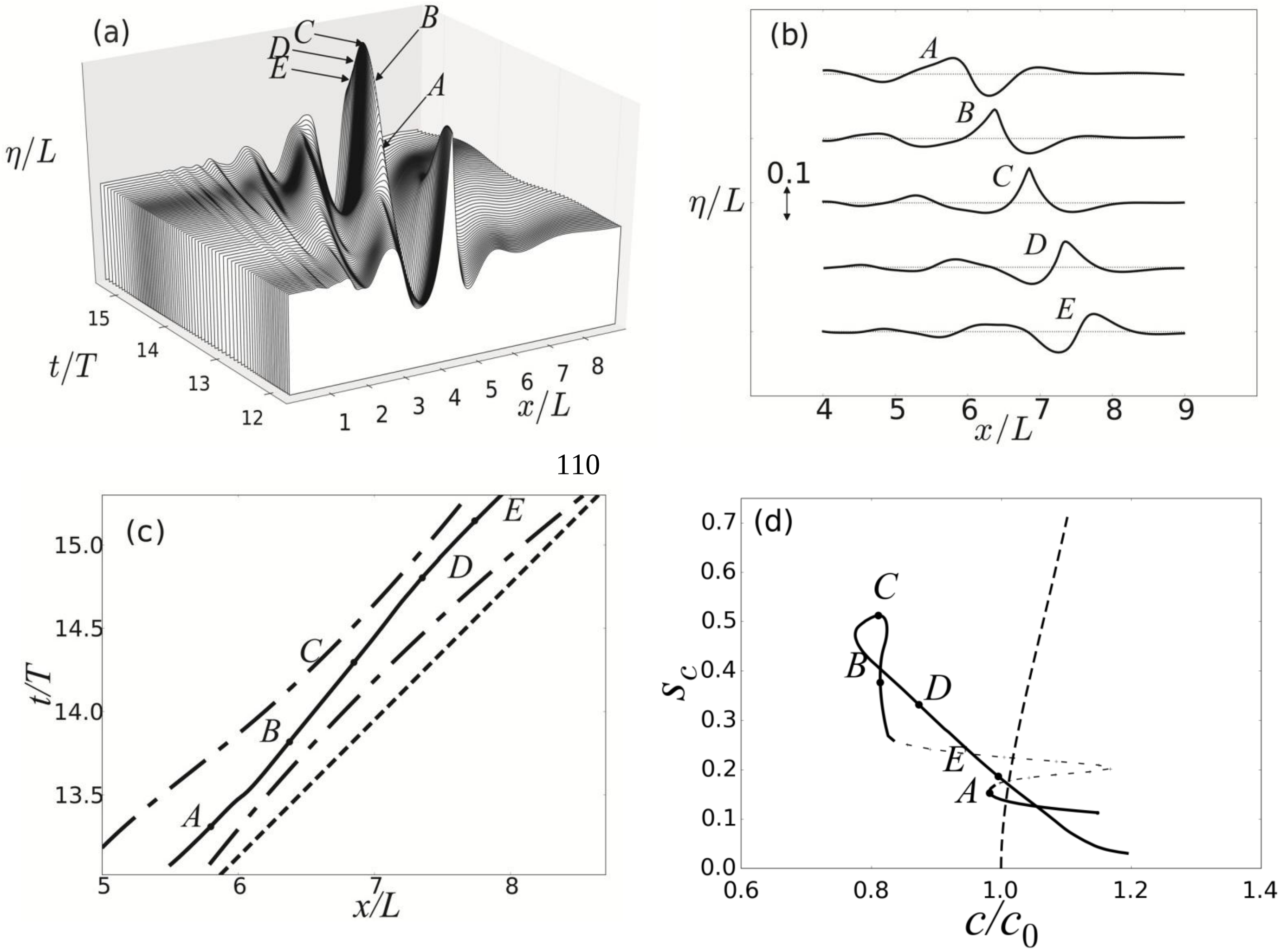

Figure 1. (a) space-time evolution diagram of a non-breaking 2D chirped wave group, moving toward the right, showing the decay of the initial tallest crest, growth of the following tallest crest and complex transitions of other developing crests. Wave properties at annotated times A-E are shown in panels (b), (c) and (d). T and L are reference carrier-wave period and wavelength scales. (b) tallest crest shapes at evolution times A-E, showing crest transition from forward-leaning through symmetry to backward-leaning (c) horizontal location of the tallest crest (solid line) versus time. The steeper slope between B and D shows the crest-speed reduction relative to c_0 (dotted line). Horizontal locations versus time of the two adjacent zero-crossings (long-short dashed lines) are also shown. (d) trajectory of the corresponding tallest crest speed c, normalized by c_0, against local crest steepness s_c defined in the text. Stokes theory prediction (1) is shown in terms of s_c (dashed line) for comparison. The apparent crest-speed surge at $s_c \approx 0.2$ is spurious, as explained in the text.

Breaking onset and speed

If the tallest wave in the group proceeds to break rather than recur, our simulations found that breaking onset occurs when this wave attains maximum steepness and close to its minimum crest speed. This can certainly explain why initial breaking wave crest speeds are observed to be O(80%) of the linear carrier-wave speed (Rapp and Melville [6]; Stansell and McFarlane [7]; Jessup and Phadnis [8]). This behavior was found in all our simulations and verified in our laboratory measurements (see Figure 2(b)).

Is the crest slowdown a nonlinear effect?

Insight on this key question is available from previous linear and weakly-nonlinear theory. For uniform, deep-water, linear gravity wavetrains, the carrier wave speed c_0 follows from the dispersion relation $\omega = (gk)^{1/2}$ and $c_0 = \omega_0/k$. However, narrow-band wave groups are characterized by non-uniformity in both space and time. Correct to $O(\nu^2)$, a local frequency can be defined (Chu and Mei [15]) as

$$\omega = (gk)^{1/2} - \beta\, a_{xx}/(ak) \qquad (2)$$

where ν is a characteristic spectral bandwidth, $\beta = dc_g/dk$, $c_g = d\omega_0/dk$ is the linear group velocity and $a(x,t)$ is the wavetrain envelope that satisfies the linear Schrödinger equation (Mei [16]). The associated local phase speed is given approximately by

$$c \approx c_0 - \beta\, a_{xx}/(ak^2). \qquad (3)$$

Equations (2), (3) and the associated relationships above show that c varies along the group and in time. Since $\beta<0$, c attains its lowest value at the envelope maximum, where the largest crest occurs ($a_{xx}<0$). The other crests and troughs in the group also experience similar local speed variations.

Furthermore, for dispersive, weakly-nonlinear unsteady wave groups, we find that the slowdown effect due to dispersion is counterbalanced by the increase in phase speed due to nonlinearity [Equation (1)], limiting the phase-velocity slowdown within the group (Fedele [17]).

Our focus on breaking-crest slowdown for large wave steepness approaching breaking onset is beyond conventional analysis methodologies. We now validate our fully-nonlinear numerical simulation findings on wave-crest slowdown against laboratory and open-ocean measurements.

Wave basin measurements

Complementary experiments were performed in a 27m x 7.75m wave basin with 0.55m water depth. Wave groups were generated at one end of the basin by a computer-controlled wave-generator comprising 13 bottom-cantilevered, flexible-plate segments. Lateral focusing was achieved by suitably setting the phase of each segment (Dalrymple [18]). A 95% absorbing beach minimized end reflections. Heights of evolving wave groups matching the simulations were measured to within ±0.5mm by a traversable in-line array of nine wave-wire probes spanning one wavelength. c_0 was calculated using linear theory from the spectrally-weighted wave frequency of the wave probe closest to the wave-generator.

Identified wave crests were tracked between the wave probe signals, their motion interpolated using cubic splining and their crest speeds extracted. An overhead one-megapixel videocamera imaged the breaking crests at 100 Hz. The imagery, corrected for lens and mounting distortion, was transformed onto a regular grid, sequential leading-edge location and lateral extent data were extracted for each breaker and their speeds determined.

Figure 2(a) shows surface profiles measured at evolution times A-E, with breaking initiation near C, for a modulating 5-wave, bi-modal breaking case. Figure 2(b) shows its crest speed trajectory. Also shown is the ensemble-mean trajectory for spilling-breaker speeds in the measured ensemble of 240 modulational and chirped 2D and 3D cases. The measurement resolution enabled resolving the crest leaning and slowing at the maximum surface elevation (C). Crest-speed oscillations observed for smaller-steepness waves (e.g. at B), are the same crest-leanings, but occurring earlier as the crest moves through the wave group. This figure confirms the reduced speeds of crests preceding breaking onset and the accompanying generic breaker slowdown.

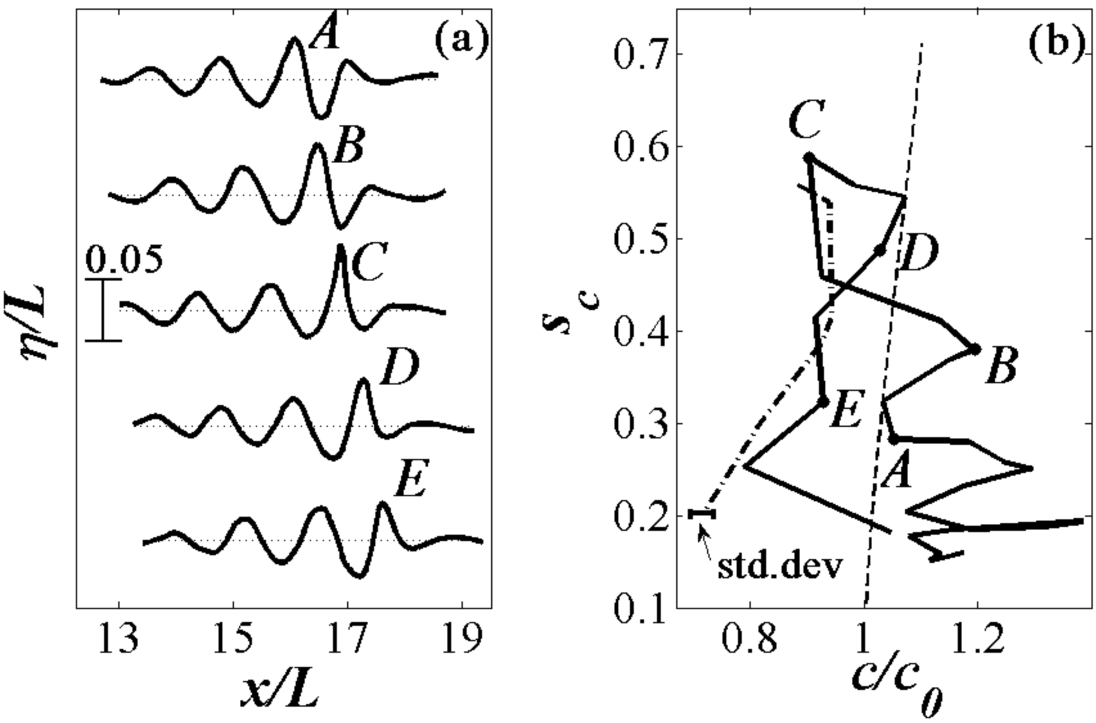

Figure 2. (a) measured surface profiles of a 5-wave, bi-modal wave packet, at times A-E, with breaking initiation at C. (b) corresponding trajectory of normalized crest speed c/c_0 of the tallest wave, against local crest steepness s_c. The ensemble-mean breaker speed trajectory is shown by the dot-dash line. The dashed line shows Stokes' prediction. Reference wave scales were L=1.09m, T=0.836 sec.

Open ocean observations

Our *Wave Acquisition Stereo System (WASS)* was deployed at the *Acqua Alta* oceanographic tower 16 km offshore from Venice in 17m water depth (Fedele et al. [19]; Benetazzo et al. [20]). *WASS* cameras were 2.5m apart, 12.5m above sea level at 70° depression angle, providing a trapezoidal field-of-view with sides increasing from 30m to 100m over a 100m fetch. The mean windspeed was 9.6 ms^{-1} with a 110 km fetch. The uni-modal wave spectrum had a significant wave height H_s=1.09m and dominant period T_p=4.59s. Most observed crests were very steep, with sporadic spilling breaking. We describe results using 21,000 frames captured at 10 Hz.

The speeds c of crests reaching maximum local steepness within the imaged area were estimated using a crest-tracking methodology, as in the wave-basin measurements. The data were filtered above 1.5 Hz to remove short riding waves. Sub-pixeling reduced quantization errors in estimating the local 3D crest position from the surface-displacement time series spaced along the wave-propagation direction. The local reference c_0 was calculated from the peak frequency of the short-term Fourier spectrum of a time series of duration D centered at the crest event, using D=120sec as a suitable record length and Doppler-corrected for the in-line 0.20 ms^{-1} mean current. We analyzed 200 dominant local wave crests with elevations $\eta > 0.3 H_s$ and local crest steepness $s_c > 0.3 (s_c)_{max}$ using the observed $(s_c)_{max}=0.45$, and determined ~12,000 evolving crest speeds from a 60-point spatial grid, with 0.5m spacing along the wave-propagation direction.

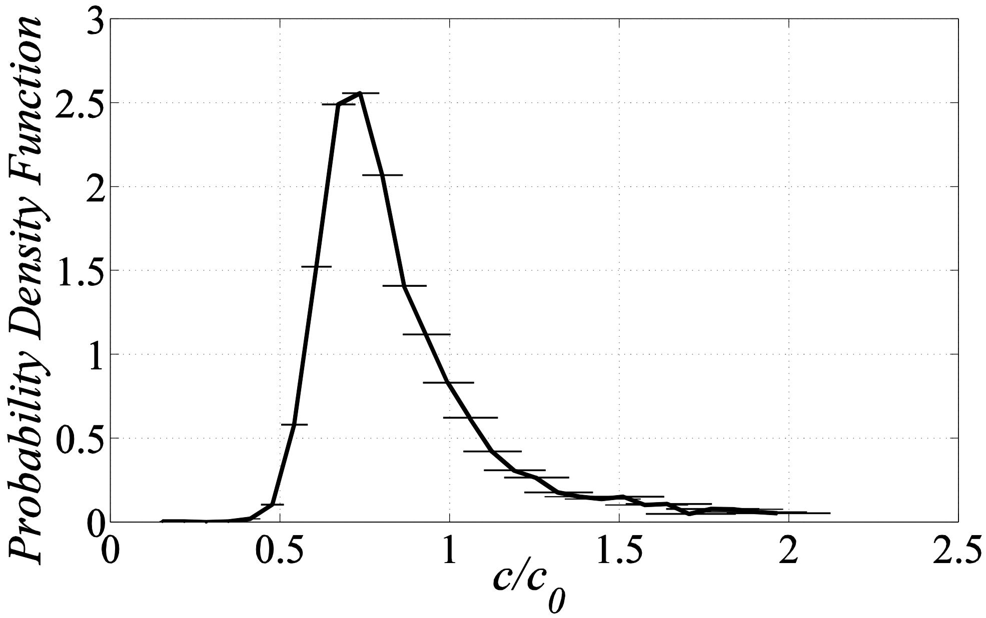

Figure 3. Probability density function of normalized crest speed c/c_0 for all crests transitioning through a maximum local crest steepness, from a 35-minute *WASS* stereo-video sequence from an ocean tower. Note the tall peak at c/c_0 ~ 0.75. Local standard error bounds are indicated.

Values of D and η were chosen so that the empirical probability density function (pdf) of c/c_0 was insensitive to changes in these parameters. Figure 3 shows the pdf, which peaks at close to $0.75c_0$. Values for $c/c_0 > 1.5$ (7% of the total ensemble) are outliers with >15% uncertainty in estimating c_0 and crest location. This figure highlights the observed crest slowdown, consistent with the nonlinear simulations and experiments described above.

Discussion and conclusions

Our study provides fundamental new insights into the behavior of chirped, bi-modal and open-ocean unsteady steep, deep-water nonlinear wave groups. We found that as carrier waves reach maximum steepness, their crests decelerate strongly (O(20%)), which results from unsteady crest sloshing modes arising from the complex interplay between nonlinearity and dispersion. This behaviour departs markedly from the speed increase with wave steepness predicted by steady-wavetrain theory.

Our findings have significant, broader consequences. For ocean waves, they explain the puzzling (O(20%)) reduced initial speed of breaking-wave crests, central to assimilating whitecap data accurately into sea-state forecast models. Parameterizations of air-sea fluxes of momentum and energy, which depend on the square and cube of the sea-surface velocity, may be modified appreciably. Atmospheric and oceanic internal waves, (Helfrich and Melville [21]), should also experience similar effects to those described here. As noted above, even weakly-nonlinear, unsteady dispersive water-wave groups described by the nonlinear Schrödinger equation (NLSE) (Zakharov [22]) exhibit crest slowdown. The NLSE is commonly used to describe wave phenomena in other natural systems (e.g. geophysical flows (Osborne [23]), nonlinear optics (Kibler et al. [24], amongst others). Exploring implications of the present findings should provide refined insights when the wave-group nonlinearity and bandwidth are beyond the validity of the NLSE.

References

1. Stokes, G.G., 1847. *Trans. Cambridge Phil. Soc.* 8, 441–455.

2. Phillips, O.M., 1985. *J. Fluid Mech.*, 156, 505-531.

3. Longuet-Higgins, M.S., 1975. *Proc. Roy. Soc.* A 342, 157-174

4. Longuet-Higgins, M.S., 1984. *Phil. Trans. R. Soc.* A 310, 219-250.

5. Tayfun, M, 1986. *J. Geophys. Res*. 91 C6:7743–7752.

6. Rapp, R.J. and Melville, W.K., 1990. *Phil. Trans. R. Soc.* A 331, 735–800.

7. Stansell, P. and MacFarlane, C., 2002. *J. Phys. Oceanogr*. 32, 1269–1283.

8. Jessup, A.T. and Phadnis, K.R., 2005. *Meas. Sci. Technol*. 16, 1961-1969.

9. Kleiss, J.M. and Melville, W.K., 2010. *J. Phys. Oceanogr.* 40, 2575–2604

10. Gemmrich, J.R., Zappa, C.J., Banner, M.L. and Morison, R.P. 2013. *J. Geophys. Res. Oceans*, In press, doi: 10.1002/jgrc.20334

11. Johannessen, T.B. and Swan, C., 2001. *Proc. Roy. Soc. Lond. A*, 457, 971-1006.

12. Johannessen, T.B. and Swan, C., 2003. *Proc. R. Soc. Lond. A*, 459, 1021-1052

13. Grilli, S., Guyenne, P. and Dias, F., 2001. *Int. J. Num. Methods Fluids*, 35, 829–867.

14. Song, J. and Banner, M.L., 2002. *J. Phys. Oceanogr*. 32, 2541–2558

15. Chu, V.H. and Mei, C.C., 1970. *J. Fluid Mech*., 41, 873-887

16. Mei, C.C., 1983. *The Applied Dynamics of Ocean Surface Waves*. Wiley-Interscience, 740pp.

17. Fedele, F., 2013. http://arxiv.org/abs/1309.0668

18. Dalrymple, R.A., 1989. *J. Hydraulic Res.* 27, 23-34.

19. Fedele, F., Benetazzo, A., Gallego, G., Shih, P.-C., Yezzi, A., Barbariol and F., Ardhuin, F., 2013. In press, http://dx.doi.org/10.1016/j.ocemod.2013.01.001

20. Benetazzo, A., Fedele, F., Gallego, G., Shih, P.C. and Yezzi, A., 2012. *Coastal Engineering*, 64, 127-138.

21. Helfrich, K.R. and Melville, W.K., 2006. *Annu. Rev. Fluid Mech*. 38:395–425.

22. Zakharov, V. E., 1968. *J. Appl. Mech. Tech. Phys*. 9, 190-194

23. Osborne, A.R., 2010. *Nonlinear Ocean Waves and the Inverse Scattering Transform.* Academic Press, ISBN: 978-0-12-528629-9, 949pp.

24. Kibler, B., Fatome, J., Finot, C., Millot, G., Genty, G., Wetzel B., Akhmediev, N., Dias F. and Dudley, J.M., 2012. *Nature Scientific Reports* 2:463, DOI: 10.1038/srep00463.

Acknowledgements

Financial support is gratefully acknowledged from the Australian Research Council through their support of Discovery Projects DP0985602, DP120101701. The WASS experiment at *Acqua Alta* was supported by Chevron (CASE-EJIP Joint Industry Project #4545093). FD was partially supported by ERC under the research project ERC-2011-AdG 290562-MULTIWAVE and SFI under the programme ERC Starter Grant - Top Up, Grant 12/ERC/E2227.

In this paper, XB identified and quantified the crest slowdown effect in his steep nonlinear wave computations. MLB made the central association with breaker slowdown and was the architect of this paper, coordinating the scientific effort. FF identified that the crest slowdown also occurs in linear wave groups. He revealed that wave group bandwidth and unsteadiness were crucial aspects of the crest slowdown, using linear/nonlinear narrow-band wave theory. MA performed the suite of laboratory wave basin experiments relating crest velocity and breaker speed. AB deployed the WASS, processed stereo data and contributed jointly with FF the WASS ocean wave crest speed analysis. WLP and FD made ongoing incisive intellectual contributions.